IET Microw. Antennas Propag., 2015, pp. 1–9. ISSN 1751-8725; doi: 10.1049/iet-map.2015.0221

Balanced Dual-Segment Cylindrical Dielectric Resonator Antennas for Ultra-Wideband Applications

A.H. Majeed, A.S. Abdullah, K.H. Sayidmarie,
R.A. Abd-Alhameed, F. Elmegri, and J.M. Noras

***Abstract*:** In this paper, balanced dual segment cylindrical dielectric antennas (CDRA) with ultra wide-band operation are reported. First a T-shaped slot and L-shaped microstrip feeding line are suggested to furnish a balanced coupling mechanism for feeding two DRAs. Performance of the proposed antenna was analyzed and optimized against the target frequency band. The proposed antenna was then modified by adding a C-shaped strip to increase the gain. The performances of both balanced antennas were characterized and optimized in terms of antenna reflection coefficient, radiation pattern, and gain. The antennas cover the frequency range from 6.4 GHz to 11.736 GHz, which is 58.7% bandwidth. A maximum gain of 2.66 dB was achieved at a frequency of 7 GHz with the first antenna, with a further 2.25 dB increase in maximum gain attained by adding the C-shaped strip. For validation, prototypes of the two antennas were fabricated and tested. The predicted and measured results showed reasonable agreement and the results confirmed good impedance bandwidth characteristics for ultra-wideband operation from both proposed balanced antennas.

Index Terms*—** *UWB, balanced antenna, Dual-segment Cylindrical Dielectric Resonator Antenna, CDRA, L-shaped feeding line.**

IET Microw. Antennas Propag., 2015, pp. 1–9. ISSN 1751-8725; doi: 10.1049/iet-map.2015.0221

1. Introduction

Ultra-wideband (UWB) antennas are key devices in many systems, such as broadband wireless communications, electronic warfare, medical imaging and radar systems. They offer many desirable features, at the same time often requiring only a simple RF front-end [1, 2]. Generally, an UWB antenna has a broad frequency range $(f_h/f_l) > 1.22$, where f_h is the upper-frequency edge and f_l is the lower frequency edge. However, the details depend on system requirements and the centre frequency of the band [2]. UWB antenna designs can be grouped into four main types. The first type has scaled structures such as Bow-Tie dipoles, biconical dipoles and log-periodic dipole arrays, while the second group is characterized by self-complementary structures featuring slot/patch combinations or spiral antennas; a traveling wave structure is utilized in the third type, as in Vivaldi antennas, and the last type features structures having multiple reflections (or resonances), and dielectric resonator antennas [3-4]. Based on the feed configuration, antennas can be categorized as balanced and unbalanced. In an unbalanced antenna, the ground plane is used as part of the radiator, with radiating currents induced on both the ground plane and the radiating element. This situation degrades the antenna's radiation characteristics and introduces losses and uncertainty in its matching. Alternatively, balanced structures can avoid this degradation in performance. In a balanced structure, currents mutually cancel their effects, with net current flowing only on the antenna radiating element and not on the ground plane, so that the performance of the antenna is not compromised [5].

Dielectric Resonator Antennas (DRAs) have been extensively studied owing to their numerous advantages such as high radiation efficiency, low weight, and small size resulting from the high permittivity of their constructing material. DRAs can be excited by various

feeding methods, such as slot, coaxial feed, microstrip line and coplanar lines [6, 7]. The DR feed line geometry has been utilized for the extension of the antenna bandwidth [8]. Other techniques to achieve UWB operation employ monopole geometries, composite DRAs using composite shapes and/or composite materials, modified ground plane shapes and use of defected ground planes [9, 10, 11, 12]. The use of dual segments of different dielectric constant fed by the same line has improved bandwidths [6, 13]. Moreover, it has been shown recently that dual similar dielectric resonators (DRs) placed asymmetrically with respect to the feeding aperture can bring an increase in bandwidth as well as more design flexibility [14, 15].

This paper introduces two designs of balanced dual-segment cylindrical DRAs for UWB applications, whose principal novelty is that they eliminate the need for a balanced feed network, i.e. a balun, as the requirements for a balanced feed and twin excitations for the two DR's are met in a single compact structure. The structure combine an inverted-T slot with two inverted-L strips to form a dipole whose arms excite the two DR's. The balanced arms, which are coupled to the dual DR elements of the antenna, are fed through a slot which is excited by an L-shaped microstrip line. As a result of the symmetric geometry, induced currents appearing on the ground plane will largely cancel mutually, minimizing net current flow on the antenna ground plane. The characteristics of these balanced antennas are analysed and optimized using the CST microwave studio suite, an electromagnetic simulator based on the finite integration technique [16].

2. Antenna Geometry

The geometry of the proposed DRA antenna is shown in Figure 1(a). The ground plane, with an area of (23×12) mm^2, is etched on the substrate bottom to constitute a copper-coated

baseboard. Two opposing L-shaped sections with a vertical L-section length f_1 = 3.4 mm, vertical L-section width W_{f2}= 1.5 mm, horizontal L-section length L_{f2} = 4.5 mm, and horizontal L-section width W_{f1} = 2.25 mm are added to the ground plane to form the balanced two-arm structure. Two cylindrical DRAs (CDRAs) of relative permittivity ε_{rdr}= 9.4, diameter D = 6.0 mm and height h = 9.0 mm are fixed symmetrically on the two opposite L-shaped sections of the ground plane. The value of tan δ for DR's was considered 0.0002 in the simulations, which a reasonable assumption for the very low loss DR's. The substrate is Rogers TMM4^{tm} with thickness t = 0.8 mm, relative permittivity ε_{rs} = 4.5, and loss tangent of 0.017, with dimensions (23×23) mm^2. As a feeding mechanism, a T-shaped slot with vertical length y = 3.5 mm, vertical width x = 1.25 mm, horizontal length s_l = 4.0 mm and horizontal width s_w = 0.35 mm is etched on the ground plane. The dimensions of the aperture influence the resonant frequency of the structure and the amount of undesired radiation in the back direction, and also determine the coupling between the radiating element and the microstrip line. The microstrip line dimensions can be calculated using empirical formulas [17]: accordingly, a 50 Ω L-shaped microstrip feed line with vertical length L_f = 10.5 mm, horizontal length L_{f3} = 6.5 mm and width W_f = 1.5 mm is used for impedance matching. At the tip of microstrip feed line, a 50 Ω coaxial SMA connector is connected for feeding microwave power.

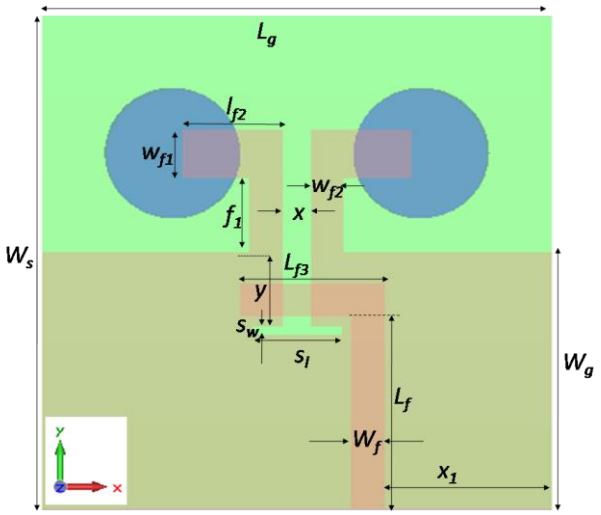

(a)

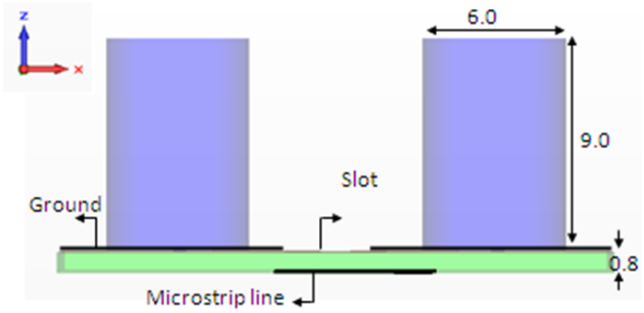

(b)

Figure 1: Balanced dual-segment cylindrical dielectric resonator antenna; (a) top view and (b) side view with design dimensions and parameters.

Figure 1 shows that the two inverted L-sections work as a half wavelength dipole that is fed by the inverted T-shaped slot. The length of the dipole is given by:

$$L_D = 2\,L_{f2} + x \qquad (1)$$

This printed dipole is not adequately thin ($L_D/\ W_{f1} \leq 10$), and thus its resonance can be considered to occur at 0.45 effective wavelength. It can be shown that the dipole resonates at a frequency f_{r1} given by:

$$f_{r1} = c/(2.22\ L_D\sqrt{\varepsilon_{re}}) \quad (2)$$

$$\varepsilon_{re} = (\varepsilon_{rs} + 1)/2 \quad (3)$$

where ε_{re} is the effective relative permittivity of the substrate.

Figure 1 also shows that the two inverted L-sections embrace an inverted-T slot having vertical length H given by:

$$H = S_w + y + f_1 + w_{f1} \quad (4)$$

Such a slot, being open-circuited at one end, can resonate at 1/4 of the effective wavelength. Using Equations 3 and 4, the resonance frequency f_{r2} can be given by:

$$f_{r2} = c/(4\ H\sqrt{\varepsilon_{re}}) \quad (5)$$

The resonant frequency of an isolated DR cylinder is calculated as [18]:

$$f_{r3} = \frac{c}{2\pi a\sqrt{\varepsilon_{rdr}}}\left[1.71 + 2\left(\frac{a}{2h}\right) + 0.1578\left(\frac{a}{2h}\right)^2\right] \quad (6)$$

Here, a = D/2 (in cm), D and h are respectively the diameter and the height of each DR, the relative permittivity of the DR material, and c is the speed of light. For the DR used here, the resonance frequency, from Equation 6, is 10.629 GHz. Thus, the expected range of frequency can be estimated using Equation 2 for the lower limit (f_{r1}) and Equation 6 for the upper limit (f_{r3}). For the design dimensions, Equation 5 gives an intermediate frequency (f_{r2}). These limits will obviously be influenced by the corresponding design parameters. The effects of various design parameters on antenna performance are investigated in the following sections.

3. Parametric Study of Dual Segment CDRD

This section reports a study to investigate how various parameters influence the response of the proposed antenna. The antenna structure was analyzed and optimized using Computer Simulation Technology (CST) microwave studio suite^{TM} 2011. The analysis was carried out by varying one parameter while holding the remaining ones fixed. The optimized dimensions are presented in Table 1. The investigations start with the effect of the T-slot parameters then proceed to explore the effects of the dimensions of the two inverted L-sections.

Table 1: Detailed parameters of the proposed antenna (all dimensions are in millimetres).

D	h	W_g	L_g	Ws	L_s	l_f	W_f	L_{f3}	x_1
6	9	12	23	23	23	10.5	1.5	6.5	7.5

The influence of the horizontal slot length s_l on the reflection coefficient is shown in Fig. 2a. With increasing horizontal slot length, there is a slight increase in impedance bandwidth, a shift in the resonance frequency towards the upwards and a slight reduction in reflection coefficient. An optimum horizontal slot length of s_l = 4 mm was chosen.

Figure 2b shows the simulated reflection coefficient of the DRA with variation of the vertical slot length (y) from 2.5 mm to 4 mm. The optimum impedance bandwidth is achieved at a vertical slot length of 3.25 mm with minimum reflection coefficient across the spectrum bandwidth.

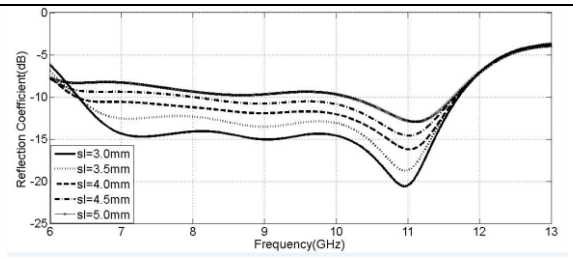

(a)

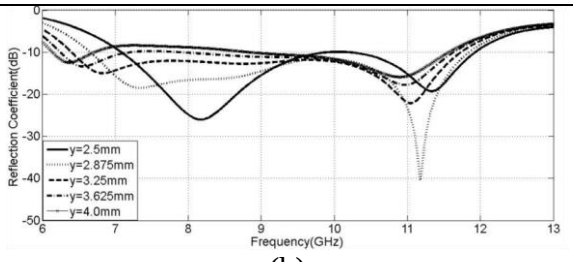

(b)

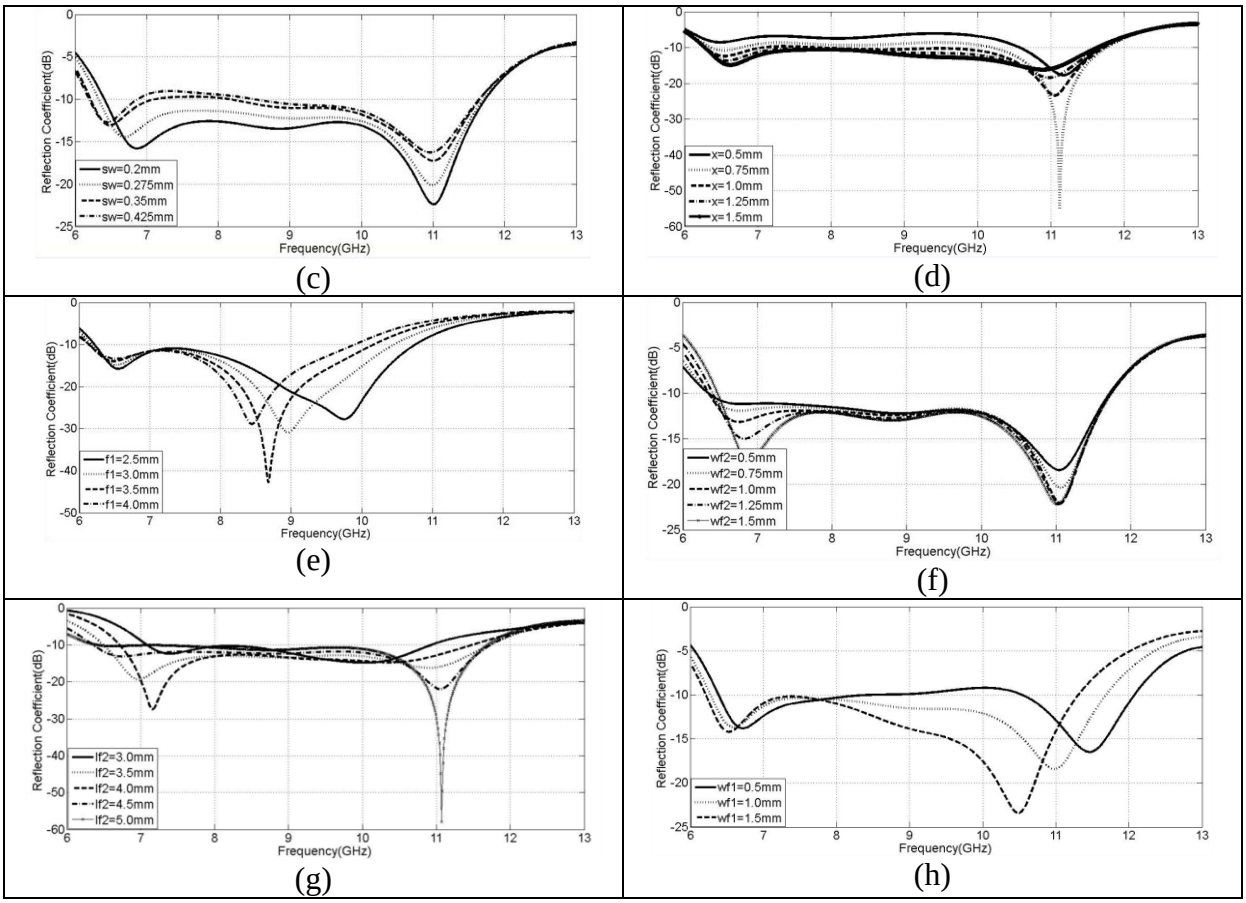

Figure 2: Simulated effects on reflection coefficient for various: (a) horizontal slot length s_l, (b) vertical slot lengths y, (c) horizontal slot width s_w ,(d) vertical slot width x ,(e) vertical L-section lengths f_1, (f) for different vertical L-section width W_{f2}, (g) horizontal L-section lengths L_{f2} and (h) horizontal L-section width W_{f1}

Figure 2c shows simulated results of the reflection coefficient of the DRA obtained by varying the horizontal slot width (s_w) of the DRA from 0.2 mm to 0.5 mm. It is clear that a slot width of 0.35 mm gives an optimum (S_{11}<-10 dB) impedance bandwidth. Figure 2d shows the simulated reflection coefficient of the DRA for varying vertical slot width, *x*, of the DRA from 0.5 mm to 1.5 mm. It is clear that a vertical slot width of 1.25 mm gives an optimum (S_{11}<-10 dB) impedance bandwidth.

Figure 2e shows the simulated reflection coefficient of the DRA with varying length of the vertical L-section, f_1, from 2.5 mm to 4.0 mm: a longer section leads to a lower value of the upper edge of the band. A vertical L-section length of 2.5 mm gives a maximum impedance bandwidth.

Figure 2f shows the simulated reflection coefficient of the DRA as the vertical L-section width (W_{f2}) is varied from 1 mm to 1.5 mm. The vertical L-section width has a slight effect on the reflection coefficient and an optimum (S_{11} < -10 dB) impedance bandwidth is achieved with W_{f2} = 1.25 mm.

Figure 2g shows the simulated reflection coefficient of the DRA for variable horizontal L-section length, L_{f2}, from 3 mm to 5 mm. The figure shows that increasing the length L_{f2} shifts the lower edge of the band towards lower frequencies. The bandwidth is also affected by the parameter L_{f2}: this can be explained by noting that the two inverted-L sections work as a $\lambda_g/2$ dipole with resonant frequency given by Equation 3. This frequency influences the lower edge of the operating bandwidth. For the dimensions shown in Table 1, taking x = 1.25 mm, L_{f2} =

4.5, and using Equation 3, the resonance frequency f_{r1} was found to be 8.023 GHz. A vertical L-section length of 4.5 mm gave a good compromise between band width and value of the reflection coefficient.

Figure 2h displays the simulated reflection coefficient of the DRA with horizontal L-section width W_{f1} varying from 1.5 mm to 3 mm, and shows that a vertical L-section width of 1.0 mm is optimum for a large impedance bandwidth.

4. Experimental Results and Discussions

To validate the proposed design, a prototype of the DRA antenna shown in Figure 1 with the optimized dimensions listed in Table 2 was fabricated and measured. The substrate parameters were ε_{rs} = 4.5, with loss tangent = 0.017, and for the DRA ε_{rdr} = 9.4. The fabricated antenna is shown in Figure 3.

Table 2: Optimum parameters of the proposed antenna (all dimensions are in millimetres).

D	h	Wg	Lg	Ws	Ls	l_f	f_1	l_{f2}	l_{f3}	W_f	W_{f1}	W_{f2}	s_w	s_l	x	x_1	y
6	*9*	*12*	*23*	*23*	*23*	*10.5*	*2.5*	*4.5*	*6.5*	*1.5*	1.0	*1.25*	0.35	4.0	1.25	7.5	3.25

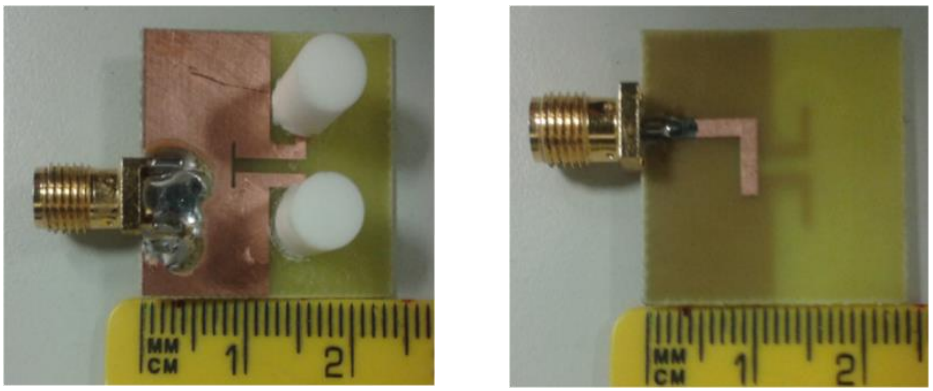

(a) (b)

Figure 3: Photo of the proposed antenna; (a) front view and (b) rear view.

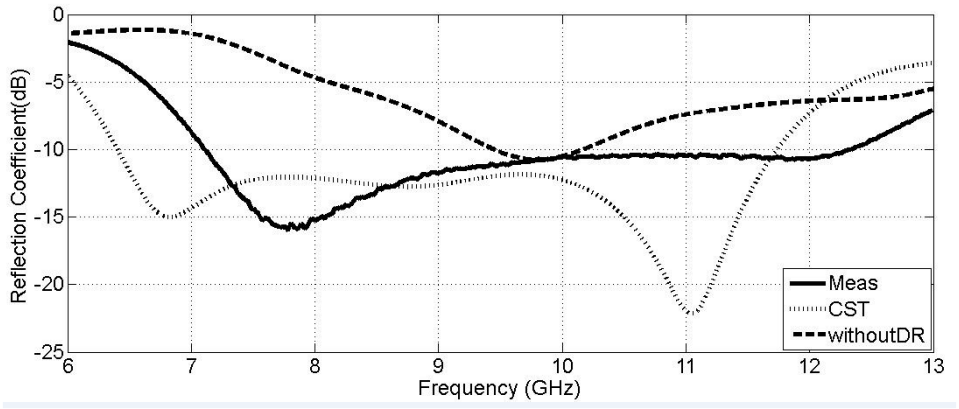

Figure 4: Simulated and measured reflection coefficients versus frequency for the proposed antenna.

The prototype was tested using an HP8510C vector network analyser, with the measured and simulated reflection coefficients shown in Figure 4. The simulated reflection coefficient of an antenna without the DRAs is shown on the same figure. The results show that the simulated antenna without two DRAs achieves an impedance matching (S_{11}< -10 dB) from 9.44 GHz to 10.16 GHz, a 7% bandwidth. Adding the two resonant posts to the dipole arms has enlarged the bandwidth range, from 6.4 GHz to 11.736 GHz, which represents a 58.7% bandwidth. The measurements results with the two DRAs show impedance matching from 7.15 GHz to 12.3 GHz, that is 52.9% bandwidth. The bandwidth achieved is higher than the 21.5% reported in [9], the 30% obtained in [12], the 32% presented in [7], while it is smaller than the 76%

obtained in [6]. The differences between the measured and simulated results, seen in a shift to higher frequency and the general increase in $S_{11,}$ can be attributed to the combined effects of the use of glue to fix the DRA and fabrication errors. Thus the addition of the two ceramic resonators has improved the reflection coefficient, and increased the impedance bandwidth.

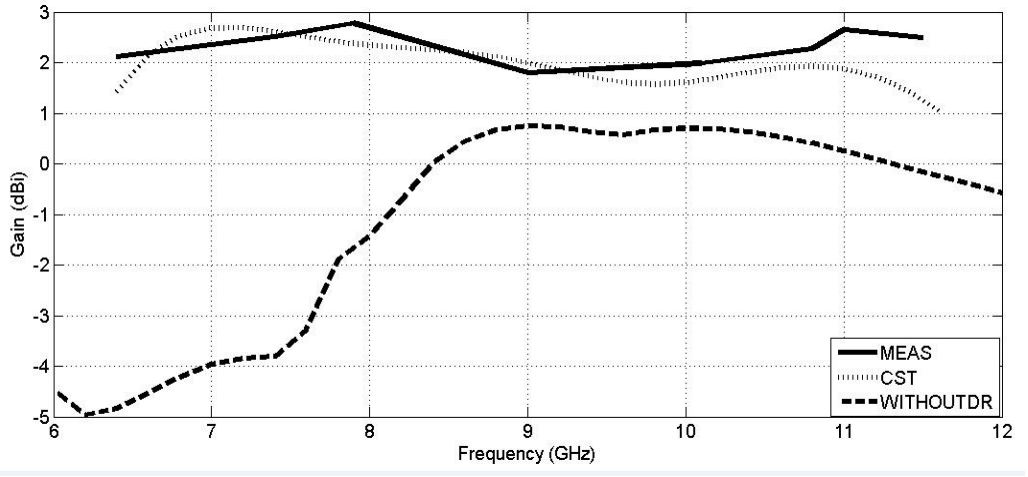

Figure 5: Measured and simulated peak gains of the proposed DRA.

Figure 5 plots the simulated peak gains of the proposed antenna with and without the DRA pair. The measured peak gain is also shown in this figure. It can be seen that the simulated antenna with DRAs has a gain that varies between 2.66 dBi and 1.86 dBi across the pass band (6.4 GHz to 11.736 GHz) and is a maximum at 7.0 GHz. The measured gain varies between 2.79 dBi and 2.63 dBi, and has a maximum at 7.89 GHz. The simulated antenna without DRAs has a gain that varies between -5.1 dBi and 0.72 dBi across the operating band, indicating that the feed/dipole structure is a weak radiator. Figure 5 also shows that the antenna gain without the DR's starts to peak up at frequency of 8.7GHz. For the data shown in Table 2, it can be shown that the resonance frequency of the inverted-T slot is 8.87GHz as predicted by Equation 5. It is clear that adding the two DRAs, which are efficient radiators, improves the gain of the antenna. The relatively small gain of the proposed antenna is attributed to its small dimensions of 23×23 mm^2: 23 mm is only 0.69 of a wavelength at a centre frequency of 9 GHz.

The results shown in Figures 2a to 2h and the experimental results of Figures 4 and 5 show that the reflection coefficient has dips at frequencies ranging from 10 GHz to 11 GHz. These are in good agreement with the resonance frequency (10.629 GHz) of the isolated DR predicted by Equation 6. The peak gain also shows a maximum at about this frequency. Although the DR is a resonating element, the wide band performance demonstrated in Figures 2a to 2h and Figures 4 and 5 can be attributed to the existence of two frequencies. The lower one, related to the $\lambda_g/2$ dipole, can be found from Equations 1 to 3. The upper frequency is controlled by the resonance frequency of the DR which is given by Equation 6.

The proposed DR antenna was also measured in the far-field using an anechoic chamber with an elevation-over-azimuth positioner, with the elevation axis coincident with the polar axis ($\theta = 0^o$) of the antenna's co-ordinate system. The azimuth drive thus generated cuts at constant ϕ. The fixed antenna (transmitting antenna) was a broadband horn (EMCO type 3115), positioned 4 m from the antenna being tested. The azimuth positioner rotated from $\theta = -180^o$ to 180^o at increments of 5^o for the selected measurement. Two pattern cuts, at $\phi = 0$ and 90^o, were taken at two selected operating frequencies, 6.8 GHz and 11 GHz, at which the matching was optimal. Figure 6 depicts the simulated and measured radiation patterns at these frequencies. It is clear that the pattern has a quasi-omnidirectional shape, and maximum antenna radiation is in the positive y-direction.

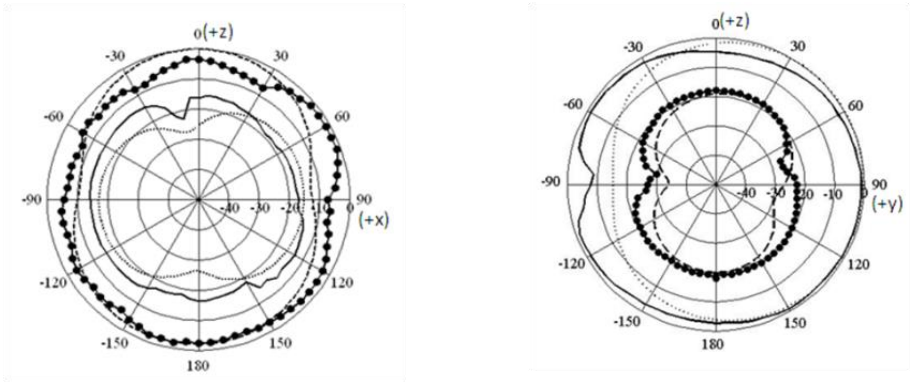

6.8 GHz

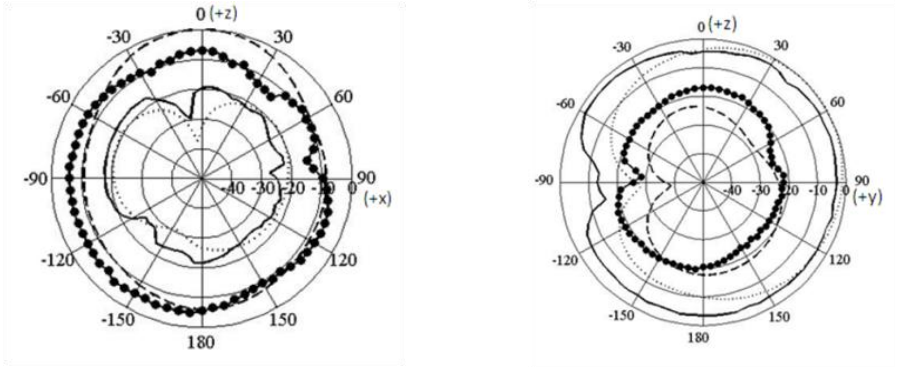

11 GHz

(a) (b)

Figure 6: Simulated and measured radiation patterns; (a) in xz plane, (b) in yz plane; simulated Eθ: dashed line, simulated Eϕ: dotted line, measured Eθ: 'o-o-o', measured Eϕ: solid line.

The distributions of the electric and magnetic fields for the optimized antenna at 6.8 GHz and 11 GHz were calculated using CST software and the results are shown in Figure 7. It is observed that the magnetic and electric field lines are parallel to the DR base, i.e. they are transverse to the DR axis. This result validates the use of Equation 6 to predict the resonance frequency of the DRs. The variations of the electric field indicate that at 11 GHz the electric field is higher at the surface of the cylinder. This finding is supported by the fact that at 6.8 GHz there is no resonance in the DRs, Equation 6 predicting the lowest mode at 10.629 GHz.

However, at 11 GHz, the DRs are very near to the resonance frequency in the $HEM_{11\delta}$ dominant mode.

5. Adding a C-shaped Strip

The proposed antenna of Fig. 1, was modified to increase its gain by adding a parasitic flipped C-shaped strip on the same side of the DRA with radius r_c and width W_c. The width of the substrate W_s was also increased as shown in Figure 8. The added strip can be considered to work as a guide to the transmitted wave leading to increased gain. The strip length is given by:

$$\text{strip length} = \frac{\text{n}^\circ}{360^\circ} \times 2\pi \,(\text{average radius of the strip}) \tag{5}$$

where n° is the sector angle of the strip.

The dimensions and position of this strip were optimized using parametric analysis. It was found that W_s = 35 mm, r_c = 7 mm, W_c = 1 mm, and a separation of y_c = 13.5 mm between the ground plane and the centre of the parasitic C-shaped strip gave the best results. The improvement in gain of the proposed antenna can be controlled by properly adjusting the parameters of the parasitic strip.

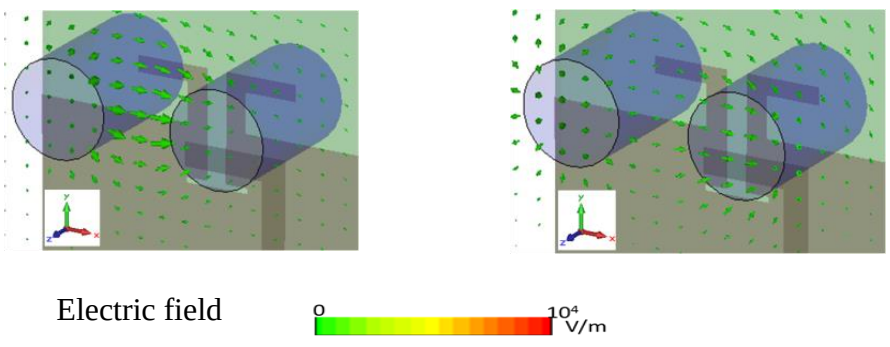

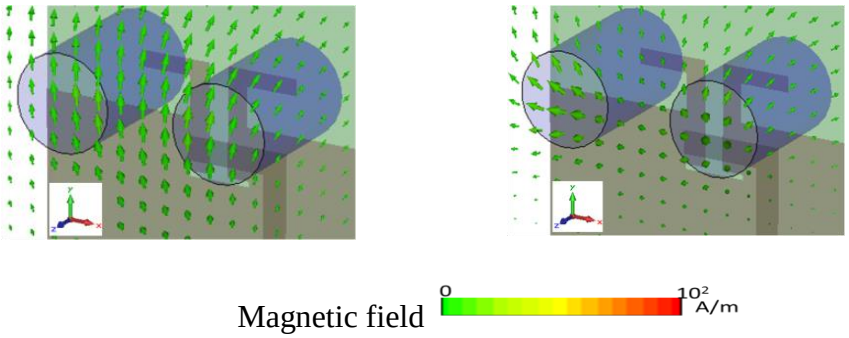

(a) (b)

Figure 7: Magnitude of electric and magnetic field distributions of the proposed T-slot fed balanced dual segment CDRA at (a) 6.8 GHz, (b) 11 GHz.

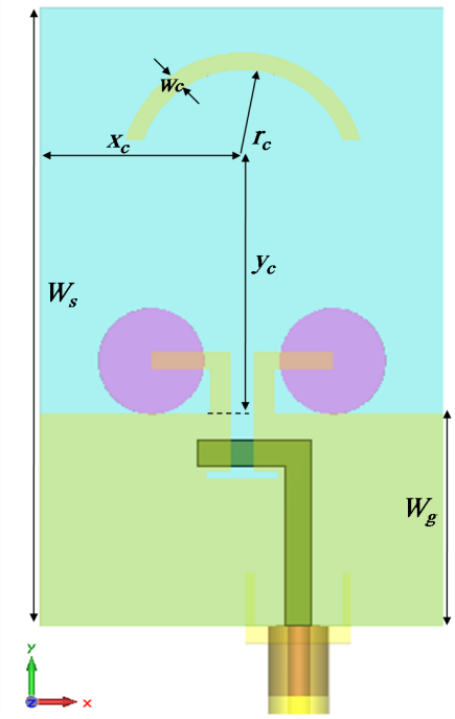

Figure 8: Geometry of the modified antenna with a C-shaped strip.

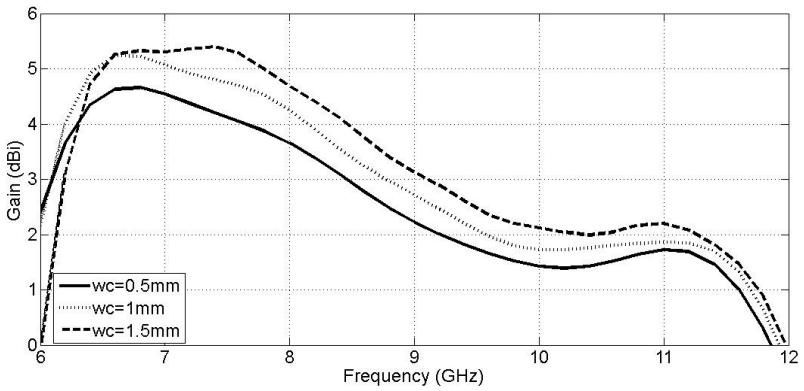

(a)

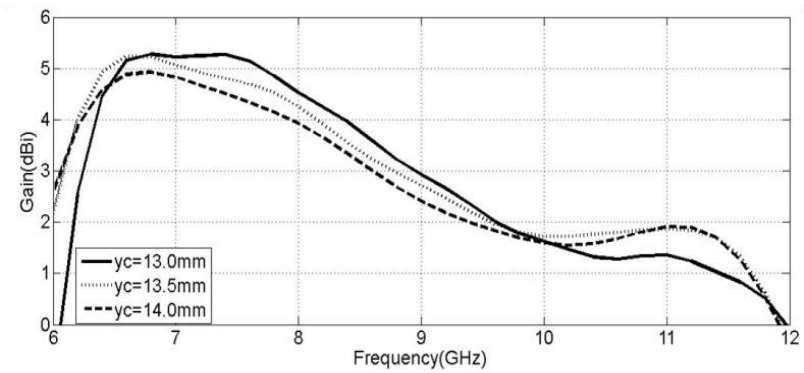

(b)

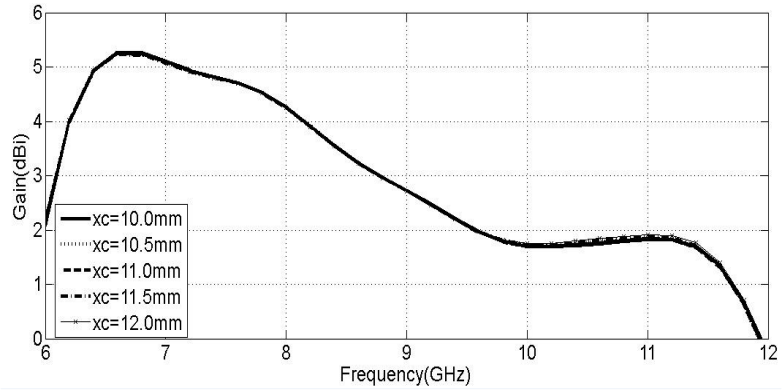

(c)

Figure 9: Simulated realized gain verses frequency for various (a) widths W_c of the C-shaped strip, (b) vertical separation between ground plane and centre of C-shaped strip y_c and (c) horizontal separations between the centre of the C-shaped strip and the edge of the substrate x_c.

Parametric Study For Modified Dual Segment CDRD

The performance of the modified antenna was analysed and optimized using the full-wave electromagnetic simulator CST Microwave Studio suit 2011. Figure 9a shows the variation of realized gain of the modified antenna with frequency for strip widths W_c from 0.5 mm to 1.5 mm. It is clear that increasing the width of the strip caused a slight increase in the realized gain in the lower edge of the frequency band and shifted the lower edge to the right.

Figure 9b shows the variation of realized gain of the modified antenna with frequency for different values of the vertical separation between ground plane and centre of the C-shaped strip y_c. There is a slight reduction in realized gain and a shift downwards at the lower end of the frequency band with increasing separation between the ground plane and the centre of the strip. However, no change towards the upper end of the frequency band was noticed.

Figure 9c shows the variation of realized gain with frequency of the modified antenna for different values of horizontal separation between the edge of the substrate and centre of the C-shaped strip x_c. The horizontal separation has a slight effect on the realized gain, thus the centre of parasitic strip is put at the centre of the horizontal axis of the substrate so that x_c = 11.5 mm.

Based on the detailed parametric studies of the flipped C-shaped strip parameters, the optimum geometry for the modified antenna was simulated, and then fabricated: Figure 10 shows a photograph of the implemented antenna. The antenna performance was measured using an HP8510C vector network analyser. The measured and simulated reflection coefficients of the proposed antenna with and without the added strip are shown in Figure 11(a). The matching properties of the antenna were only slightly affected by the addition of the strip as this is relatively far from the DRs.

The measured and simulated gains, for the designs with and without the C-shaped strip, are shown in Figure 11(b). It can be seen adding the strip has increased the antenna gain by about 2.25 dB at the lower half of the operation band, while there is marginal improvement in the upper half of the band. The C-shaped strip with a radius of 7 mm, width of 1 mm and a strip angle of 140° has an average physical length of 18.326 mm. This strip length can resonate at half wavelength as well as unity wavelength. For the substrate used, the two resonating modes are at 4.94 GHz and 9.87 GHz. However, the gain of the antenna will be affected by the two L-section dipoles as well as the C-shaped strip. Former results of Figure 5 show that the dipole has a peak gain at about 7 GHz and 8 GHz for the simulation and measured results. The C-shaped strip has a resonance at a predicted frequency of 9.87 GHz. It should be noted here that the obtained gain is a result of the combined effects of many factors: the added strip,

the two DRs, and the two arms of the inverted L-shaped lines that feed the two DRs. Another effect to be considered is the separation distance (y_c) between the active radiators (formed by the dipole and two DR's) and the parasitic radiator (C-strip). As Figure 9b shows, this separation can affect the gain by about 1 dB. The combined effect on the antenna has resulted in a maximum gain which shows peaking at lower frequencies, around 6.5 to 7 GHz for the CST results and 7.5 to 8 GHz for the measured results.

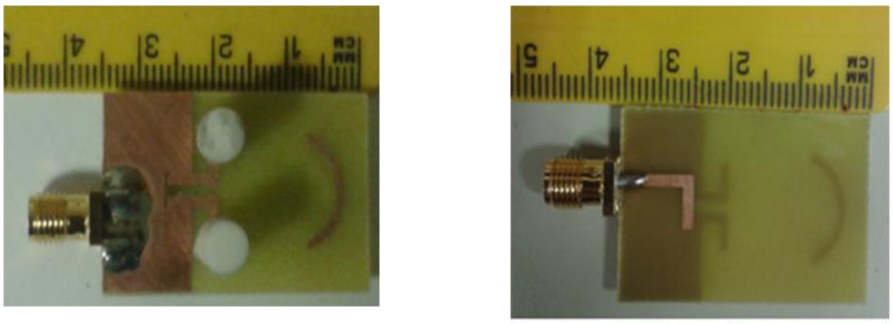

(a) (b)

Figure 10: Fabricated antenna (a) front view and (b) rear view.

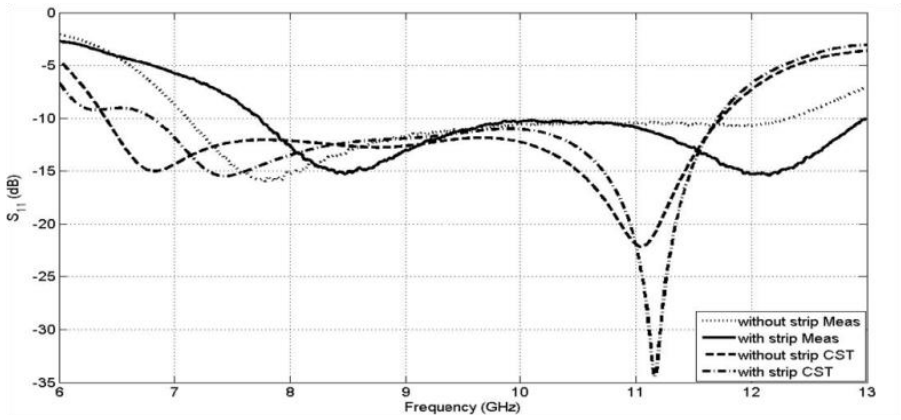

(a)

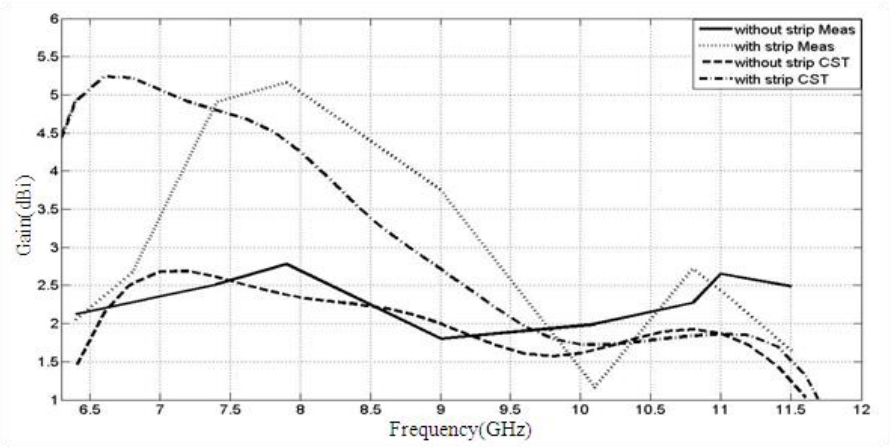

(b)

Figure 11: Simulated and measured (a) reflection coefficient and (b) gain versus frequency for the proposed antenna with strip and without strip.

6. Conclusion

A DRA consisting of balanced dual segment CDRs excited by two L-section feeding dipole is proposed. The dipole is fed by a T-shaped slot that is aperture-coupled to a microstrip L-shaped feeding line. Parametric studies have been carried out to optimize the antenna design. The designed antenna offered good impedance bandwidth from 6.4 GHz to 11.734 GHz (58.7% for S11 $\leq$ -10 dB), and also a maximum gain of 2.66 dB_i at 7 GHz. Modifying the design, by adding a C-shaped strip and increasing the width of the substrate, resulted in a 2.24 dB increase in the maximum gain while maintaining nearly the same impedance bandwidth. The measurements showed good agreement between simulated and measured results. The measured radiation patterns, and peak gains of the proposed antennas validate use of the proposed antennas for UWB applications. As the proposed antennas have three resonating elements, three formulas were derived to guide the design and to explain the performance.

The formulas gave good agreement with the CST simulations and the measured experimental results.

ACKNOWLEDGEMENT

The authors gratefully acknowledge the support of the Engineering and Physical Sciences Research Council (EPSRC) in the UK under grant EP/E022936, and in addition the support of the Iraqi Ministry of Higher Education and Scientific Research.

References

1. H. G. Schantz, "A Brief History of UWB Antennas", IEEE Aerospace and Electronic Systems Magazine, Vol. 19, No. 4, pp. 22-26, 2004.
2. W. Wiesbeck, G. Adamiuk, C. Sturm, "Basic Properties and Design Principles of UWB Antennas", Proceedings of the IEEE, Vol. 97, No. 2, pp. 372-385, 2009.
3. D. Nyberg, P.-S. Kildal, J. Carlsson, "Effects of Intrinsic Radiation Q On Mismatch Factor Of Three Types Of Small Antennas: Single-Resonance, Gradual-Transition And Cascaded-Resonance Types", IET Microwaves, Antennas & Propagation, Vol. 4, No. 1, pp. 83-90, 2010.
4. Yang and A. Kishk, "A Novel Low-Profile Compact Directional Ultra-Wideband Antenna: The Self Grounded Bow-Tie Antenna", IEEE Trans. on Antennas and Propagation, Vol. 60, pp. 1214-1220, 2012.
5. R. A. Abd-Alhameed, P. S. Excell, R. A. K. Khalil, and J. Mustafa, "SAR and Radiation Performance Of Balanced And Unbalanced Mobile Antennas Using A Hybrid Computational Electromagnetic Formulation," IEEE Proceedings; Science, Measurement and Technology special issue on Computational Electromagnetics, Vol. 151, pp. 440-444, 2004.
6. P. Rezaei, M. Hakkak and K. Forooaghi, "Design Of Wideband Dielectric Resonator Antenna With A Two Segment Structure," Progress in Electromagnetics Research, PIER 66, pp. 111-124, 2006.

7. A. A. Kishk, R. Chair, and K. F. Lee, “Broadband Dielectric Resonator Antennas Excited By L-Shaped Probe,” IEEE Trans. on Antennas and Propagation, Vol. 54, No. 8, pp. 2182–2189, 2006.
8. P.V. Bijumon, S.K. Menon, M.N. Suma, M.T. Sebastian and P. Mohanan," Broadband Cylindrical Dielectric Resonator Antenna Excited By Modified Microstrip Line", Electronics Letters 31st March 2005, No. 7, Vol. 41.
9. M. Khalily, M. K. A. Rahim, A. A. Kishk, S. Danesh,"Wideband P-Shaped Dielectric Resonator Antenna", Radioengineering, No. 1, April 2013, Vol. 22, pp. 281-285.
10. D. Soren, R. Ghatak, R. K. Mishra, and D. R. Poddar, "Dielectric Resonator Antennas: Designs And Advances”, Progress In Electromagnetics Research B, Vol. 60, pp. 195-213, 2014.
11. Yongmei Pan; Kwok Wa Leung, "Wideband Circularly Polarized Trapezoidal Dielectric Resonator Antenna," Antennas and Wireless Propagation Letters, IEEE, Vol. 9, pp. 588-591, 2010.
12. C.S. De Young, S.A. Long, "Wideband Cylindrical and Rectangular Dielectric Resonator Antennas," Antennas and Wireless Propagation Letters, IEEE, vol. 5, no. 1, pp. 426-429, Dec. 2006.
13. A. Rashidian and D. M. Klymyshyn, “On The Two Segmented And High Aspect Ratio Rectangular Dielectric Resonator Antennas For Bandwidth Enhancement And Miniaturization,” IEEE Trans. Antennas and Propagation, vol. 57, No. 9, pp. 2775-2780, 2009.
14. A. H. Majeed, A. S. Abdullah, F. Elmegri, K. H. Sayidmarie, R. A. Abd- Alhameed, and J. M. Noras," Aperture-Coupled Asymmetric Dielectric Resonators Antenna for

Wideband Applications", IEEE Antennas And Wireless Propagation Letters, Vol. 13, pp. 927-930, 2014.

15. A.H. Majeed, A.S. Abdullah, F. Elmegri, E.M. Ibrahim, K.H. Sayidmarie, R.A. Abd-Alhameed, "Rectangular Slot Fed Asymmetric Cylindrical Dielectric Resonators Antenna for Wideband Applications", Loughborough Antennas and Propagation Conference LAPC 2014, 8-11 Nov. 2014, pp. 244-248.
16. “CST: Computer simulation technology based on FDTD method", CST Computer Simulation Technology AG, 2011.
17. D.M. Pozar, “Microwave Engineering”, 2nd edition, John Wiley & Sons, New York, 1998.
18. A. Kishk, et al., “Slot Excitation of the Dielectric Disk Radiator,” IEEE Transactions on Antenna and Propagations, Vol. 43. No. 2, Feb. 1995.